Nanoscale Advances

Accepted Manuscript

This article can be cited before page numbers have been issued, to do this please use: N. Rostami, M. R. Naimi-Jamal and M. G. Dekamin, *Nanoscale Adv.*, 2026, DOI: 10.1039/D5NA00544B.

ROYAL SOCIETY OF CHEMISTRY

rsc.li/nanoscale-advances

Nanoscale Advances

View Article Online
DOI: 10.1039/D5NA00544B

ARTICLE

A pH-sensitive β-cyclodextrin-modified periodic mesoporous organosilica hybrid nanomaterial for co-delivery of paclitaxel and curcumin in lung cancer

Negin Rostami,[a,b] Mohammad Reza Naimi-Jamal*[§a] and Mohammad G. Dekamin*[§b]

Received 20th May 2025,

Accepted 00th xxxx 2025

DOI: 10.1039/x0xx00000x

In this study, a novel β-cyclodextrin grafted to 3-aminopropyl and incorporated in the periodic mesoporous organosilica structure (β-CD-APTS-PMO) was prepared via a co-condensation and sequential integration strategy. At first, β-CD-APTS-PMO hybrid nanomaterial was characterized using various techniques including FESEM, FT-IR and EDS spectroscopy, elemental mapping, XRD, TGA, BET, and potential zeta. The β-CD-APTS-PMO hybrid nanomaterial with surface area of 284.35 m^2g^{-1} and average pore diameter of 4.9 nm was developed to evaluate its in vitro antitumor activity. Paclitaxel (PTX) and curcumin (CUR) were successfully co-encapsulated at a pre-optimized ratio in β-CD-APTS-PMO with high encapsulation efficiency (CUR: 90.2 ± 0.56%, PTX: 87.4 ± 0.12%). Paclitaxel and curcumin co-loaded β-CD-APTS-PMO demonstates sustained-release properties in vitro. However, the drug release profile results demonstrated that CUR was released much faster than PTX. The release of CUR in advance would allow effective chemosensitization of cancer cells, which in turn would increase the therapeutic efficacy of PTX. The results of MTT study indicate that paclitaxel and curcumin co-loaded β-CD-APTS-PMO had a better anticancer effect than free paclitaxel or curcumin. These results indicate that β-CD-APTS-PMO is a promising candidate for the lung cancer combination therapy.

Introduction

In recent years, periodic mesoporous organosilicas (PMOs) that combine the properties of both organic and inorganic materials have been widely employed to develop new biomedical solutions. [1-3] This type of mesoporous material synthesized by incorporating organic bridging groups into the silica framework during the sol-gel process which can be tailored by choosing specific organic precursors and synthesis conditions.[4-7] The specific properties of PMOs have made them versatile candidates for the fields of gas storage and CO_2 capture,[8] sensing,[9, 10] drug delivery[11, 12] and catalytic activity.[13-15]

The organic moieties of PMOs can be designed to enhance targeting capabilities, drug stability, and biocompatibility.[16] As well as, the silica-based inorganic framework can provide large surface area and well-defined mesoporous structure for high drug loading capacity, controlled drug release and protection of drugs.[17, 18] The versatility, tunability, and biocompatibility of PMOs make them highly promising in the field of drug delivery.[19, 20] PMOs have been investigated as carriers for the delivery of anticancer drugs with promising therapeutic properties.[21] In this regard, PMOs can encapsulate drug molecules within their mesoporous structure, enhancing its biocompatibility and biodegradability.[22] This encapsulation protects drug composition from enzymatic degradation, oxidation, and interactions with biological components, thereby increasing its bioavailability.[23] Additionally, the mesoporous structure of PMOs allows for the gradual release of drugs, ensuring a prolonged therapeutic effect.[24] The release rate can be tailored by adjusting the pore size, surface chemistry and composition of the PMOs.[25, 26] Some recent examples of PMOs that have been used for drug delivery include HPMO for paclitaxel,[27] GA-PMO-15 for 5-fluorouracil (5-Fu) and ibuprofen (IBU),[28] MON for curcumin,[29] His-PMO for paclitaxel,[30] Cys-PMO for Doxorubicin,[31] AGu@PEG1500-PMO for Cas9-sgRNA ribonucleoprotein,[32] B-PMO for paclitaxel,[33] DMONs-PDA/CNC for paclitaxel,[34] and MCNs for curcumin.[35]

β-cyclodextrin (β-CD), a cyclic oligosaccharide composed of glucose units with a lot of O-H groups, can be create hybrid nanomaterials with enhanced properties and applications.[36, 37] β-CD has a hydrophobic cavity that can encapsulate guest molecules of appropriate size and shape.[38-40] More importantly, by incorporating β-CD into PMO, β-CD can create a host-guest system within the mesopores, allowing for the controlled encapsulation and release of guest molecules.[41] This property is particularly useful for drug delivery, where β-CD-APTS-PMO can serve as carrier for hydrophobic drugs.[42] Furthermore, β-CD can improve the solubility and stability of hydrophobic guest molecules, including poorly soluble drugs.[43, 44]

According to statistics, cancer is among the deadliest diseases and the deaths caused by lung cancer total more than 18% of

[a]*Research Laboratory of Green Organic Synthesis and Polymers, Department of Chemistry, Iran University of Science and Technology, P.O. Box 16846–13114, Tehran, Iran. *Email:* naimi@iust.ac.ir.
[b]*Pharmaceutical and Heterocyclic Compounds Research Laboratory, Department of Chemistry, Iran University of Science and Technology, Tehran, 16846-13114, Iran. *Email:* mdekamin@iust.ac.ir.
§ Two authors have an equal contribution to this article.
† Footnotes relating to the title and/or authors should appear here.
Supplementary Information available: [details of any supplementary information available should be included here]. See DOI: 10.1039/x0xx00000x

View Article Online
DOI: 10.1039/D5NA00544B

the total cancer deaths in worldwide.[45, 46] However, chemotherapy based on anticancer small molecule cytotoxic drugs is the most common approach.[47-49] The results of recent research show that combining anticancer drugs with curcumin (CUR) in a single delivery system not only reduces the required dose of the drug, but also increases the therapeutic effect and reduces side effects.[50-52]

Co-delivery of paclitaxel and curcumin refers to the simultaneous delivery of both drugs in a combined formulation or delivery system.[53] Paclitaxel is a chemotherapy drug commonly used to treat various types of cancer, including breast,[54] lung,[55] and ovarian cancer.[56, 57] Curcumin is a natural compound found in turmeric, which has been shown to possess anti-inflammatory and anticancer properties.[58, 59] The co-delivery of paclitaxel (PTX) and curcumin has attracted significant attention in recent years due to the potential synergistic effects of two drugs.[50, 60] According to studies, curcumin can enhance the anticancer activity of paclitaxel and reduce its side effects.[61, 62] Several approaches have been explored for the co-delivery of paclitaxel and curcumin, including liposomes,[50] nanoparticles,[63, 64] micelles,[51] mesoporous silica nanoparticles[65] and polymeric systems.[66] These delivery systems can encapsulate both drugs and control their release kinetics, allowing for simultaneous and sustained delivery to the target site.[67] The advantages of co-delivery include enhanced therapeutic efficacy, reduced drug resistance, and minimized systemic toxicity.[68-70]

Overall, the co-delivery of paclitaxel and curcumin holds great potential for enhancing cancer treatment outcomes. However, further research and clinical trials are needed to optimize the co-delivery systems, determine the optimal drug ratios, and validate their efficacy and safety in a clinical setting. Furthermore, the incorporation of β-cyclodextrin into PMO creates hybrid materials with enhanced host-guest interactions, improved solubility, and controlled release capabilities. These features make β-CD-APTS-PMO attractive for applications such molecular absorption and release and drug delivery. In continuation of our previous studies about PMO-based nanomaterials as well as drug delivery systems, this work aims to optimize the synthesis, explore new functionalization, and broaden the applications of β-CD-APTS-PMO for the synergistic co-delivery of paclitaxel and curcumin in lung cancer therapy.[49, 71-73]

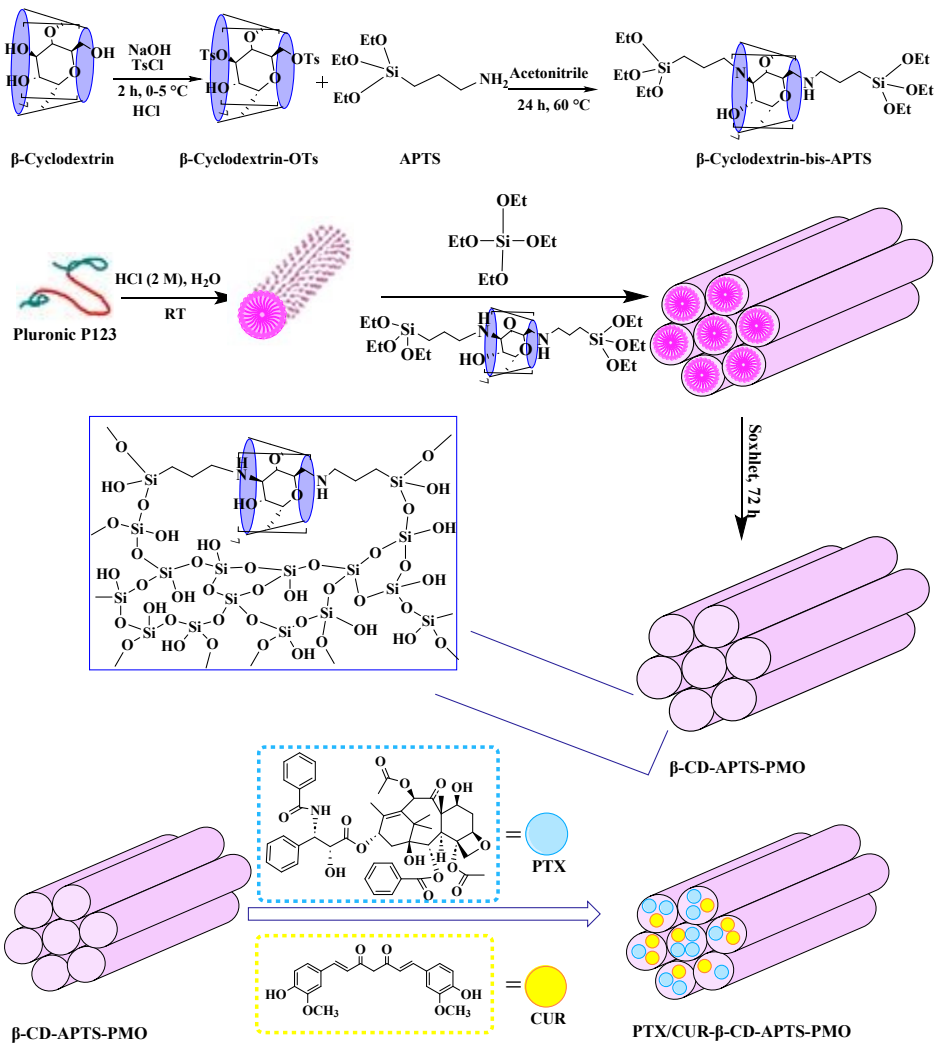

Scheme 1. Schematic synthesis and fabrication process of β-CD-APTS-PMO and co-delivery of PTX and CUR.

View Article Online
DOI: 10.1039/D5NA00544B

Experimental

Materials and methods

β-cyclodextrin (β-CD, 98%), 4-toluenesulfonyl chloride (TsCl) and (3-aminopropyl)triethoxysilane (APTS, 99%), Pluronic P123 and Tetraethoxysilane (TEOS) were purchased from Merck or Aldrich and used as received for preparation of β-cyclodextrin-bis-APTS (β-CD-bis-APTS). Paclitaxel (MW = 853.906 g/mol), curcumin (MW = 368.37 g/mol) and 3-(4,5-dimethyl-thiazol-2-yl)-2,5-diphenyltetrazolium bromide (MTT) were purchased from E-Merck Products. Characterization of the new B-CD-APTS-PMO was performed by FTIR (Shimadzu 8400S spectrometer), FESEM (MIRA II TESCAN instrument), EDX (TESCAN4992), BET (ASAP™ 2020 Micromeritics), TGA (Bahr Company STA 504) and XRD (Bruker D8 advance). ^{1}H NMR spectra of the β-CD-OTs and β-CD-bis-APTS precursor were recorded at 500 MHz in DMSO-d_6 using a Varian-INOVA spectrometer. UV-Vis spectra were measured on a Shimadzu UV-2550PC Spectrophotometer. Zeta potential of the nanocarriers and drug loaded nanocarriers were determined using an instrument from Particlemetrix Zeta-Sizer analyzer. Spectral data were compared with those obtained from authentic samples or reported in the literature.

Preparation of the β-cyclodextrin-OTs

β-CD have a lot of OH groups that must functionalized with amino group via two steps by reference to the previous literatures.[74] the first step is tosylation and second is amination.[73] In brief, β-cyclodextrin (β-CD, 5.0 g) were dissolved in DI water and stirred at 0 – 4 °C in an ice and cold-water bath and NaOH (6.0 M, 3.0 mL) was added drop by drop until the solution was entirely clear. Then, 4-toluenesulfonyl chloride (TsCl, 1.5 g) dissolved in acetonitrile (1 mL) was added dropwise over 5 min and reacted under vigorous stirring for 2 h. The solution containing tosylated β-CD (β-CD-OTs) was neutralized about pH 6 – 7 by using HCl (6.0 M). The white solid product was collected by filtration and recrystallized from hot water and dried for 6 h, at room temperature (MW = 1289 g.mol^{-1}, Yield: 55%). The β-CD-OTs was characterized by means of FTIR and ^{1}H NMR spectroscopy.

FTIR (KBr disk) υ: 3380, 2927, 1637, 1365, 1157, 1027, 839, 757 cm^{-1}; ^{1}H NMR (500 MHz, DMSO-d_6): δ (ppm) 7.73 (d, J = 8.2 Hz, 4H), 7.45 (d, J = 8.2 Hz, 4H), 4.82 (s, 1H, CH), 4.47 (br, 1H, OH), 3.64 (m, 6H, CH or CH_2), 2.42 (s, 6H, CH_3).

Preparation of the β-CD-bis-APTS precursor

At first, β-CD-OTs (1.289 g, 1.0 mmol) was dispersed in 20 mL of acetonitrile for 30 min at room temperature. Then, APTS (2 mmol, 0.442 g) was added and stirred for 24 h at 60 °C to form a white gel containing β-CD-bis-APTS. Eventually, the acetonitrile solvent was evaporated under vacuum in a rotary evaporator. The formation of product was confirmed by FT-IR spectroscopy (**Fig. 2c**). The β-CD-bis-APTS precursor was characterized by means of FTIR and ^{1}H NMR spectroscopy.

FTIR (KBr disk) υ: 3422, 3360, 2927, 1637, 1577, 1316, 1126, 1033, 760 cm^{-1}; ^{1}H NMR (500 MHz, DMSO-d_6): δ (ppm) 5.86 (s, 2H, NH), 4.82 (s, 1H, CH), 4.69 (br, 1H, OH), 3.80 (m, 6H, CH or CH_2), 3.12 (q, J = 7.2 Hz, 12H, CH_2), 2.78 (t, J = 7.6 Hz, 4H, –NH–CH_2–), 2.63 (m, 4H, –CH_2–), 1.23 (t, J = 7.2 Hz, 18H, CH_3), 0.76 (t, J = 7.6 Hz, 4H, Si–CH_2–).

Preparation of the β-CD-APTS-PMO hybrid nanomaterials

A solution of 1.28 g of Pluronic P123 and 48 mL HCl (2.0 M) in DI water (12 mL) was prepared under stirring conditions for 2 h at room temperature. Then, β-CD-bis-APTS (0.55 g) was added slowly to the mixture with TEOS (2.8 mL) and stirring for 24 h at 50 °C and held afterward for 24 h at 80 °C. Eventually, the β-CD-APTS-PMO hybrid nanomaterial was collected by filtration, washed with DI water, and dried at 50 °C. The P123 extraction was carried out in ethanol (96%, 180 mL) and HCl (12.0 M, 6 mL) using a soxhelet apparatus at 100 °C for 72 h. The final β-CD-APTS-PMO product was collected by filtration, washed with DI water and dried at 60 °C.

In vitro loading curcumin and paclitaxel on the β-CD-APTS-PMO

For preparing β-CD-APTS-PMO-PTX and β-CD-APTS-PMO-CUR, PTX (20 mL of 500 µg/mL solution in ethanol) and CUR (20 mL of 500 µg/mL dissolved in ethanol) were mixed with different amounts of β-CD-APTS-PMO (0.15 g, 0.2 g and 0.25 g), respectively, and stirred 24 h at room temperature. Also, in the combination form, solutions containing PTX (20 mL of 500 µg/mL solution in ethanol) and CUR (20 mL of 500 µg/mL solution in ethanol) were mixed together and evaluated with different amounts of β-CD-APTS-PMO (0.15 g, 0.2 g and 0.25 g) (**Table S2**). The drug-loaded nanocarriers were separated by centrifugation, washed with distillated water and dried using a vacuum oven at 30 °C. Unbound drugs concentration of the supernatant was determined by UV-Vis standard curves of PTX and CUR at λ_{max} = 218 nm and λ_{max} = 428 nm, respectively (**Fig. 1**). The loading efficiency of drugs was calculated according to the initial concentration of PTX and CUR and the concentration of the unloaded remaining solution by the following equations (Eq. 1, 2).

$$\%\ \textbf{Loading capacity} = \frac{\mathbf{wi} - \mathbf{wr}}{\mathbf{whn}} \times \mathbf{100} \qquad \textbf{(Eq. 1)}$$

$$\%\ \textbf{Entrapment efficiency} = \frac{\mathbf{wi} - \mathbf{w\,r}}{\mathbf{wi}} \times \mathbf{100} \qquad \textbf{(Eq. 2)}$$

where wi, wr, and whn represent the initial drug weight, residual drug weight, and hybrid nanomaterial weight, respectively.

pH-Sensitive release study

The in vitro drugs-release kinetics research of PTX and CUR from PTX-β-CD-APTS-PMO, CUR-β-CD-APTS-PMO and PTX/CUR-β-CD-APTS-PMO was monitored in PBS at two different pH values (7.4 and 5.5). At predetermined time intervals, 1.0 mL of released medium was withdrawn for testing and replenished with equivalent fresh PBS buffers to keep the final volume constant. The concentration of PTX and CUR released from PTX-β-CD-APTS-PMO, CUR-β-CD-APTS-PMO and PTX/CUR-β-CD-APTS-PMO were detected by UV-Vis spectrophotometry at λ_{max} = 218 nm and λ_{max} = 428 nm, respectively. Calibration standards for PBS (pH = 5.5 and pH = 7.4) were containing a low percentage of Tween 80 (0.5%), which significantly enhances the solubility of both PTX and Cur in the aqueous release medium. Each sample in the release kinetics study was conducted in triplicate.

In drug delivery, release kinetics models are mathematical equations that describe how quickly and in what pattern a drug is released from a delivery system. The CUR and PTX release mechanism were investigated by analyzing drug release kinetics using common mathematical models: Zero-order (**Eq. 3**), First-order (**Eq. 4**), Higuchi (**Eq. 5**), and Korsmeyer-Peppas (**Eq. 6**).

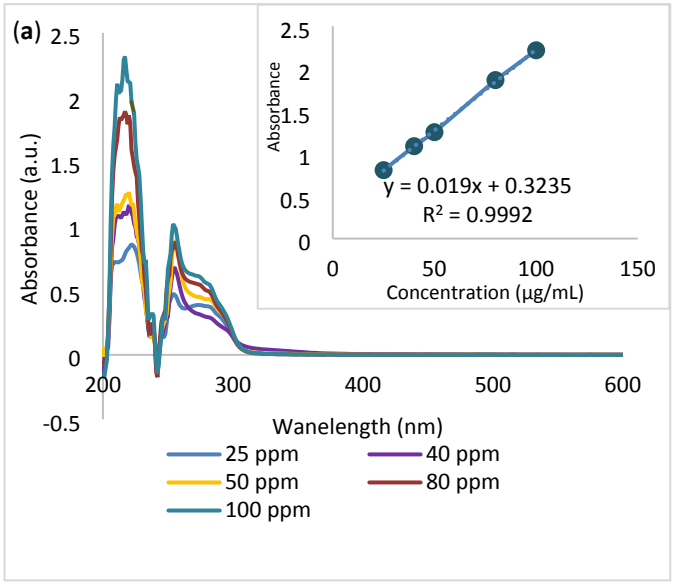

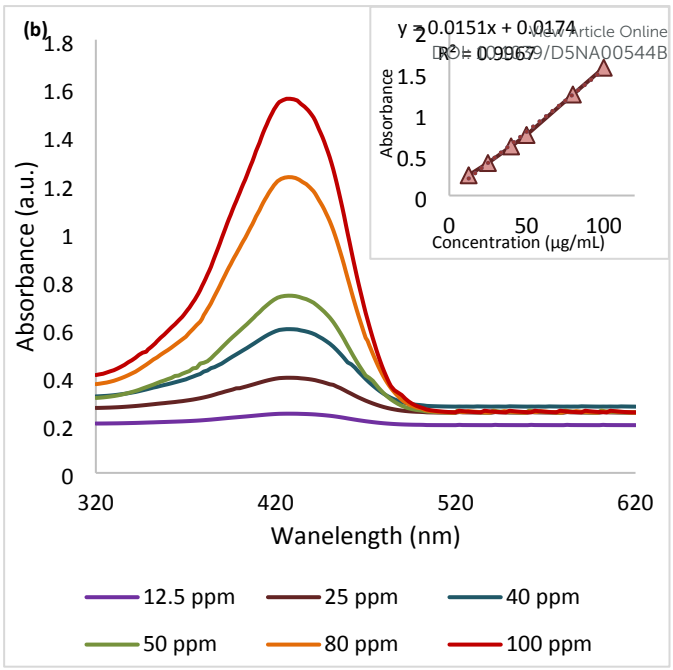

Fig. 1 Standard calibration curve of paclitaxel (a) and curcumin (b).

$Q = k_0 t$ **(Eq. 3)**

$LnQ = LnQ_0 - k_1 t$ **(Eq. 4)**

$Q = kHt^{1/2}$ **(Eq. 5)**

$LnQ = nLnt + Lnkp$ **(Eq. 6)**

Cell cytotoxicity (MTT test)

A549 (a lung adenocarcinoma epithelial cell line) was sourced from the NCBI (National Cell Bank of Iran, Pasteur Institute of Iran, Tehran). The cells were maintained in DMEM (Dulbecco's Modified Eagle Medium), a standard growth medium, which was enriched with 10 % Fetal Bovine Serum (FBS) and 1 % penicillin-streptomycin (pen/strep) for essential nutrients and contamination control. The cells were maintained in a controlled environment of 37 °C, 5 % CO_2 and 95 % humidity, and the cells were transferred into a new cell culture plate. The culture medium for the nearly confluent cells was refreshed every three days. DMEM Medium, FBS and Pen-strep, were purchased from Sigma-Aldrich (USA).

In order to confirm the effect of drugs and drugs-loaded nanocarriers, cell cytotoxicity was measured by MTT assay. Briefly, A549 cell line (human lung cancer cell) were seeded in 96-well plate at a cell density of 5,000 cells per well in 200 µl DMEM medium and then cultured overnight for fully attaching. In the following, cells were treated with different concentrations of drugs and drugs-loaded nanocarriers and incubated for 48 h. Media without any drugs and nanocarriers were added to the control wells. Absorbance was recorded at 570 nm.

View Article Online
DOI: 10.1039/D5NA00544B

Results and discussion

Fourier transform infrared spectroscopy (FTIR analysis)

FTIR spectroscopy was employed to characterize vibrational stretching modes of the β-CD (a), β-CD-OTs (b), β-CD-bis-APTS (c) and β-CD-APTS-PMO (d). The peak at 3100 - 3600 cm^{-1} is associated with O-H groups and symmetric and asymmetric N-H stretching vibration. The C–H aliphatic vibration bands are shown at 2920 - 2930 cm^{-1}. In the β-CD-OTs spectrum, the sharp peak at 1365 cm^{-1} is a sign of the presence of S=O of tosyl group, which was not observed in the β-CD-bis-APTS spectrum and indicates that tosyl group has been left. The spectra of β-CD-APTS-PMO showed characteristic bands at 1073 and 952 cm^{-1} correspond to the asymmetric and symmetric stretching vibrations of Si-O-Si bonds. O-H bending vibration are clearly observed at 1637 cm^{-1}. The FT-IR spectra confirmed the successfully preparation of β-CD-APTS-PMO.

Field emission scanning electron microscopy (FESEM)

The morphology of the β-CD-bis-APTS and β-CD-APTS-PMO was studied by FESEM and depicted in **Fig. 2**. Pure β-CD have a plate-like crystalline structure.[75] After modification with APTS, the β-CD-bis-APTS shows a significant change in its morphology. The β-CD-bis-APTS form larger, irregularly shaped clusters on the surface of β-CD. This change confirms the successful modification of β-CD with the APTS linkers. FESEM images of β-CD-APTS-PMO indicated that it includes interwoven tubular particles with 48.5 – 52.7 nm in width. In addition, the uniform arrangement of mesopores and tubular mesochannels are very appropriate to drug delivery purposes and drug loading capability.

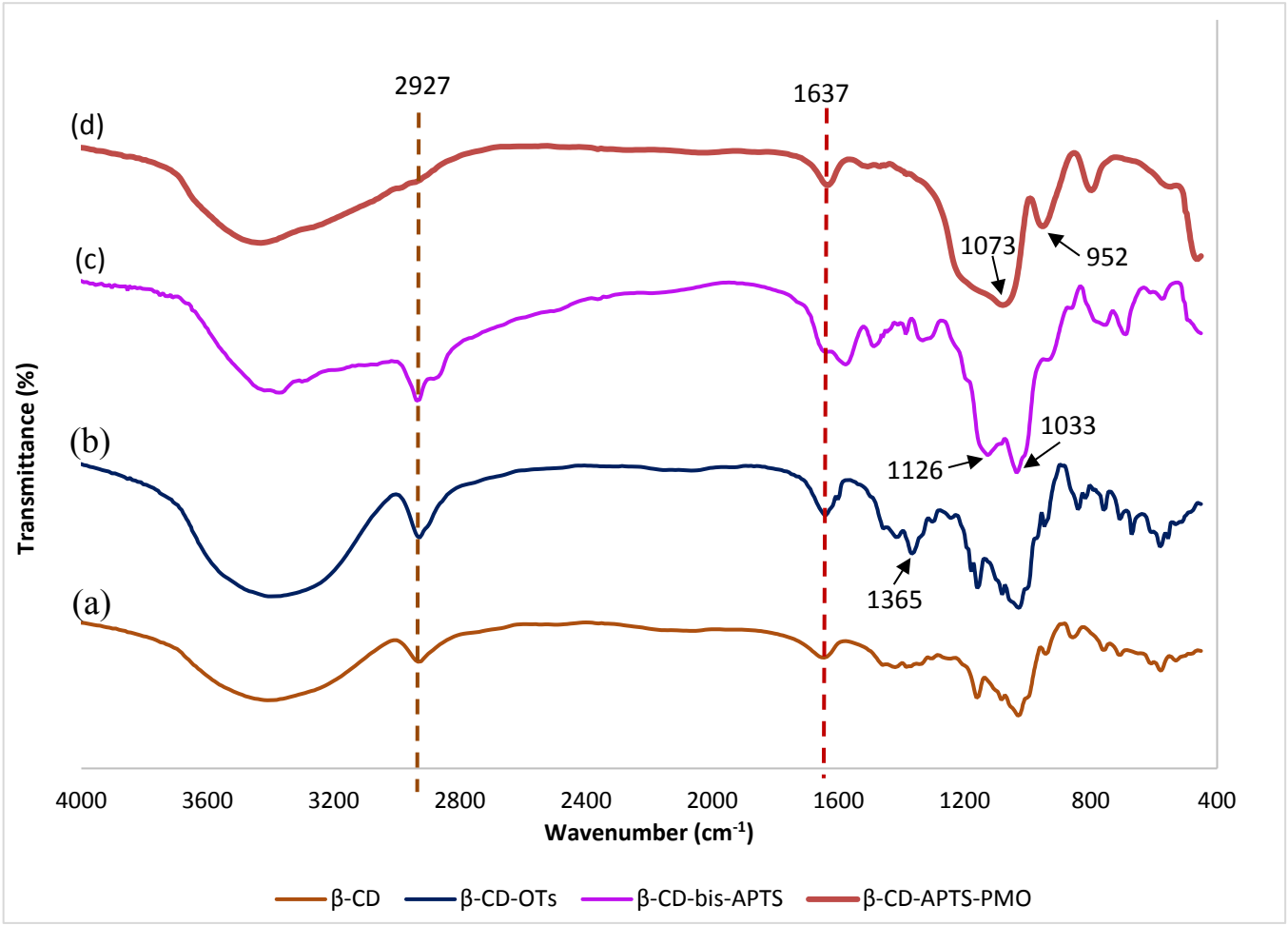

Fig. 2 FTIR spectra of the β-CD (a), β-CD-OTs (b), β-CD-bis-APTS (c) and β-CD-APTS-PMO (d).

Energy Dispersive X-Ray Analysis

EDX was used to identify the elemental composition of β-CD-OTS (a), β-CD-bis-APTS (b) and β-CD-APTS-PMO (c). EDX analysis of β-CD-OTs confirmed the presence of C, O and S elements. The presence of C, O, N and Si in Elemental analysis of β-CD-bis-APTS confirms that APTS is well connected to β-CD-OTs and toluene sulfonyl chloride was

removed. As expected, The EDX analysis of β-CD-APTS-PMO reveals the presence of C, N, O and Si. As well, the elemental mapping of β-CD-APTS-PMO indicated uniform dispersion of C, N, O and Si elements (**Fig. 4c**).

View Article Online
DOI: 10.1039/D5NA00544B

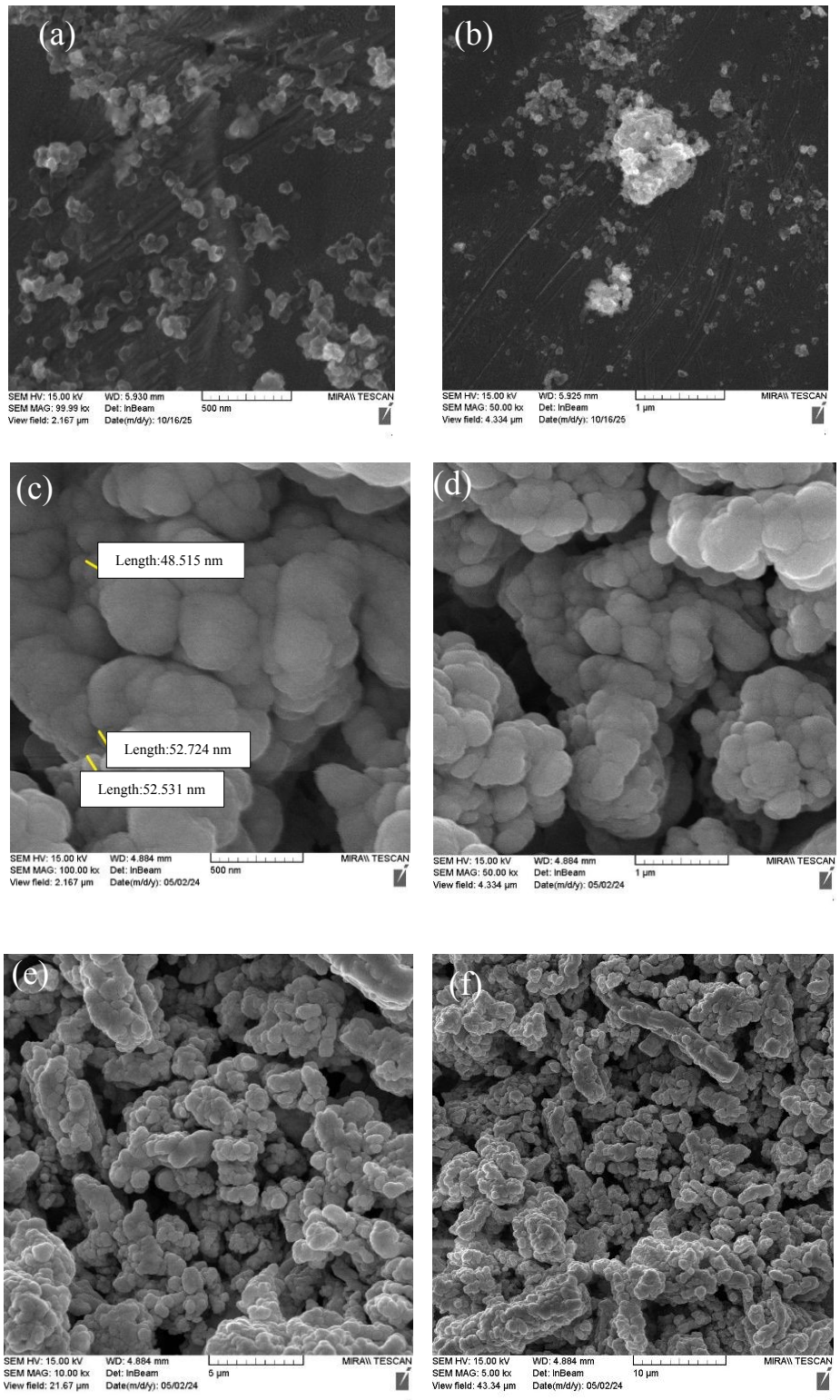

Fig. 3 FESEM images of β-CD-bis-APTS (a-b) and β-CD-APTS-PMO with different magnifications (c-f).

Nanoscale Advances

View Article Online
DOI: 10.1039/D5NA00544B

ARTICLE

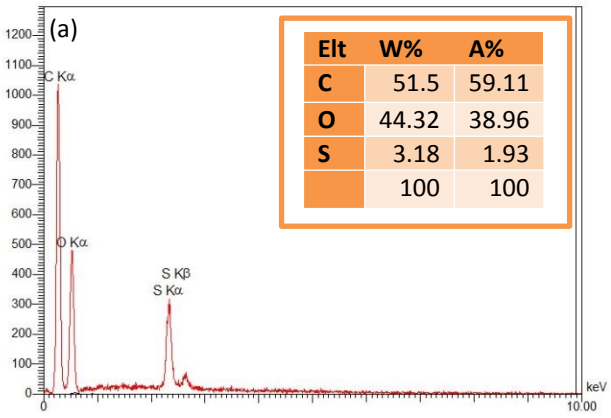

Elt	W%	A%
C	51.5	59.11
O	44.32	38.96
S	3.18	1.93
	100	100

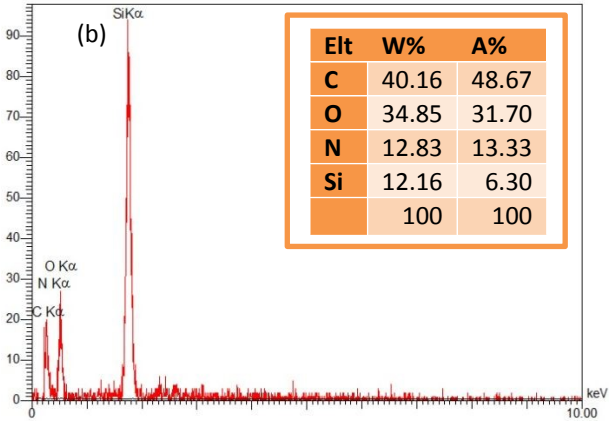

Elt	W%	A%
C	40.16	48.67
O	34.85	31.70
N	12.83	13.33
Si	12.16	6.30
	100	100

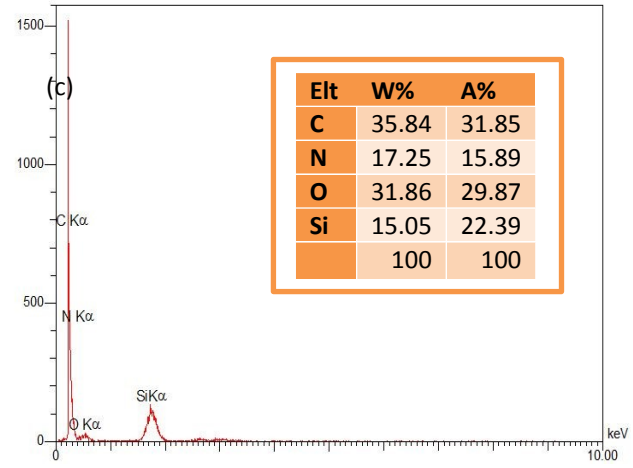

Elt	W%	A%
C	35.84	31.85
N	17.25	15.89
O	31.86	29.87
Si	15.05	22.39
	100	100

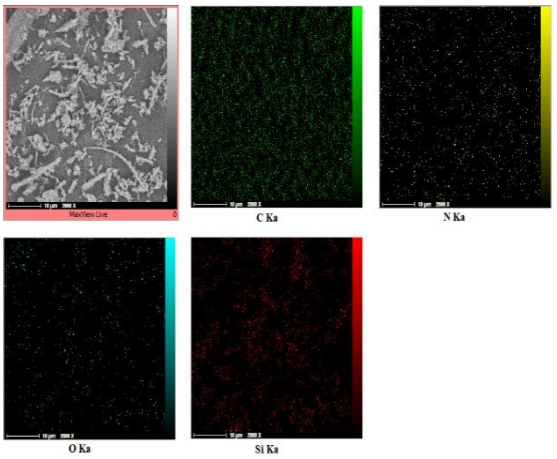

Fig. 4 EDX analysis of β-CD-OTs (a), β-CD-bis-APTS (b) and β-CD-APTS-PMO (c), and elemental mapping of β-CD-APTS-PMO (d).

Thermal gravimetric analysis (TGA) the β-CD-APTS-PMO

The stability of β-CD, β-CD-bis-APTS and β-CD-APTS-PMO was analysed by thermogravimetric analysis as displayed in **Fig. 5**. The thermogram of β-CD showed the mass loss in two stages. In the first stage, about 16% weight loss occurred between 50 - 130 °C, which is related to adsorbed water molecules. Furthermore, about 70% weight loss occurs at between 300 - 500 °C in the later stage, which is associated with the decomposition of the glucopyranose units in the structure of initial β-CD or subsequent macrocycles.[76] On the other hand, the TGA curve of the β-CD-bis-APTS reveals a multi-step thermal decomposition process as the temperature is increased from ambient conditions to 800 °C. An initial weight loss of approximately 6% is observed in the temperature range of 50 - 150 °C, which is corresponded to the evaporation of absorbed water molecules and potentially any residual solvent trapped within the structure. The second step shows a broad mass loss of about 15% between 150 – 450 °C, which is attributed to the thermal degradation of the organic components, especially the initial decomposition of the β-CD glucose units. The final major thermal decomposition occurs between 450 - 650 °C, showing a substantial weight loss of approximately 24%. This represents the major degradation of the β-cyclodextrin macrocycle (comprising glucopyranose units) as well as the complete thermal breakdown of the remaining organic components of the APTS linker. Eventually, the remaining mass of about 53% at 800 °C is related to the inorganic residue, which is characteristic of silane-containing materials. This residue is primarily composed of silica (SiO_2), formed by the thermal oxidation of the silane groups (APTS). The main mass loss steps confirm the thermal degradation of the organic β-CD and silane components. TGA curve of β-CD-APTS-PMO indicates that about 15% weight loss between 50 - 150 °C can be related to the

elimination of adsorbed solvent or water molecules into its pores. In addition, weight loss about 5% between 150 - 300 °C can be assigned to decomposition of amounts of the unextracted surfactant (P123). In the last step, at the temperature of 300 to 800 °C, the β-CD bridges are decomposed. Simultaneously, the silanol groups on the surface of silica moiety are condensed to siloxane ones, which is reflected by remaining of about 60% initial weight of the β-CD-APTS-PM.

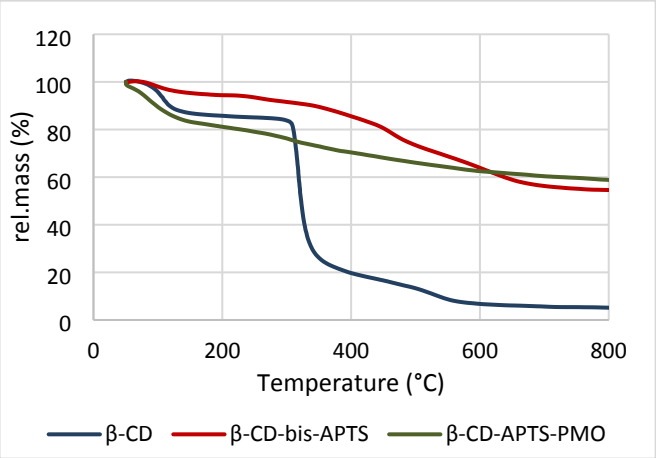

Fig. 5 Thermogravimetric curve of the β-CD, β-CD-bis-APTS and β-CD-APTS-PMO.

X-Ray diffraction (XRD) pattern of the β-CD-APTS-PMO

XRD patterns of β-CD-bis-APTS, β-CD-APTS-PMO, CUR/PTX-β-CD-APTS-PMO are shown in **Fig. 6**. The presence of some sharp peaks in the low-angel XRD pattern of β-CD-bis-APTS suggests that its units are arranged in a highly periodic fashion to create a structured mesophase. Furthermore, the wide-angle XRD pattern of β-CD-bis-APTS shows an amorphous structure with a significantly reduced degree of crystallinity compared to the pure β-CD. Indeed, the characteristic sharp peaks of crystalline β-CD are disappeared and significantly broadened with reduced intensities. A large hump, cantered at 2θ = 15 – 25°, dominated the wide-angle XRD pattern. This indicates that the β-CD-bis-APTS possesses a low degree of long-range order and is significantly amorphous and a more disordered structure. The disappearance or broadening of the sharp β-CD peaks suggests that the covalent attachment of the APTS moiety has distorted its regular crystal packing macrocycles. In general, silica-based mesoporous structures have two characteristic peaks in their XRD patterns: a low-angle peak at 2θ = 1.1 – 1.7° (to confirm their mesostructure characteristic) and a wide-angle peak at 2θ = 20 – 30° (to confirm their crystallinity), respectively.[7] In the low-angle XRD patterns of β-CD-APTS-PMO, the characteristic mesostructure peak was observed at 2θ = 1.51°. In addition, in the wide-angle XRD pattern, a broad peak was observed at 2θ = 17 – 30°, which proves the formation of the β-CD-APTS-PMO. Consequently, the XRD pattern of a functionalized mesoporous material such as CUR/PTX-β-CD-APTS-PMO is typically analysed in two main regions to confirm its structure and the state of the loaded drugs: Low-angle XRD and wide-angle XRD (to confirm the crystallinity as well as successful drug loading). The low-angle XRD pattern of the CUR/PTX-β-CD-APTS-PMO provides crucial evidence regarding its highly ordered mesostructure characteristic. Specifically, the low-angle XRD pattern of the CUR/PTX-β-CD-APTS-PMO shows three distinct and sharp diffraction peaks in the 2θ range below 10, which is the characteristic region for probing the mesoscale order. A slight shift or reduction in the intensity of these peaks in the CUR/PTX-β-CD-APTS-PMO compared to the β-CD-APTS-PMO would indicate successful drug loading within the pores. This result suggests that the organic encapsulated drugs occupy the mesochannels, slightly altering the diffraction properties of the pore walls without destroying the overall structural order.

(a)

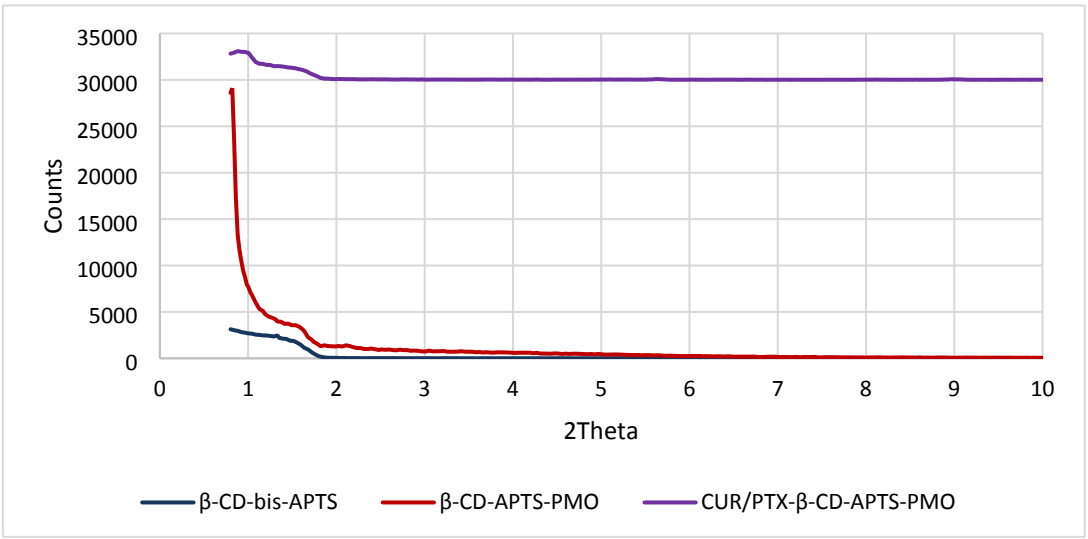

View Article Online
DOI: 10.1039/D5NA00544B

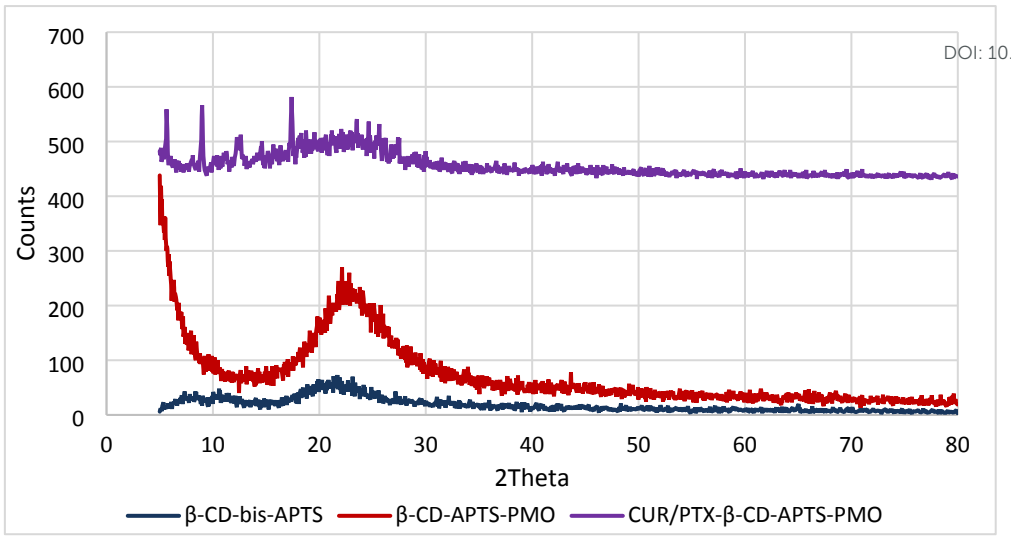

Fig. 6 (a) Low-angle and (b) wide-angle XRD pattern of the β-CD-bis-APTS, β-CD-APTS-PMO, CUR/PTX-β-CD-APTS-PMO.

Brunauer-Emmett-Teller analysis (BET)

N_2 adsorption-desorption isotherms of β-CD-bis-APTS and β-CD-APTS-PMO and the corresponding BJH pore size distribution curve of β-CD-APTS-PMO is represented in **Fig. 7**. In general, PMOs showed the typical type IV isotherms with a H1 hysteresis loop, characteristic of mesoporous materials with uniform cylindrical pore.[77] BET surface area, average pore diameter and total pore volume of β-CD-bis-APTS and β-CD-APTS-PMO are approximately 93.667 and 284.35 $m^2. g^{-1}$, 1.9289 and 4.9 nm, 12.52 and 0.3505 $cm^3.g^{-1}$, respectively (**Table S1**). The pore-size distribution has its maximum at 4.6 nm, as shown in the **Fig. 7b**.

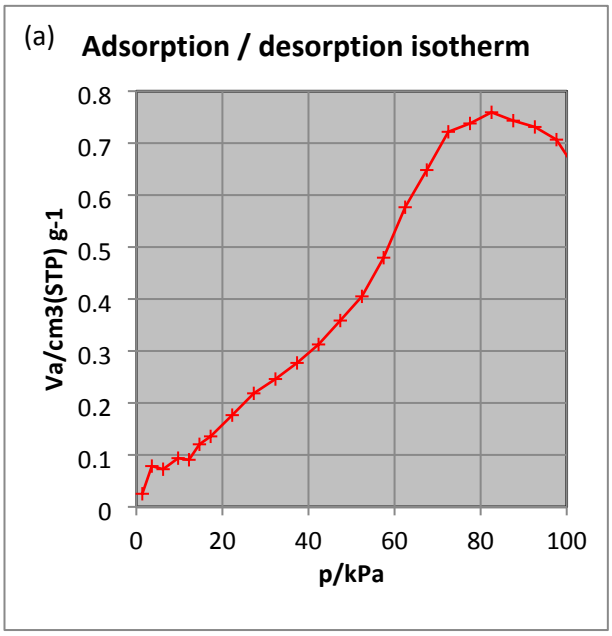

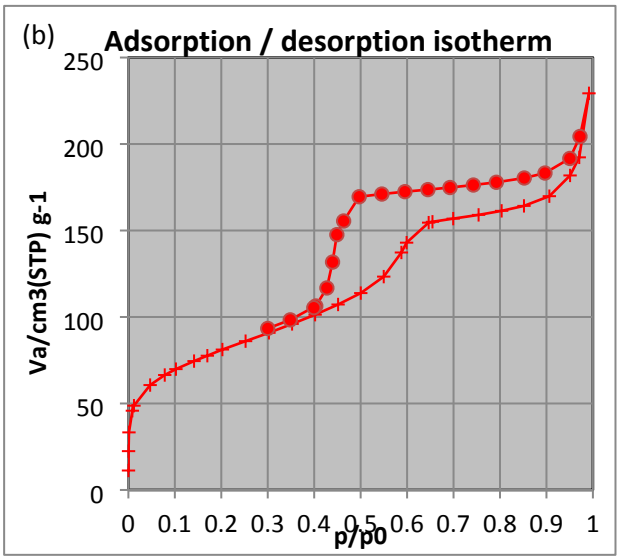

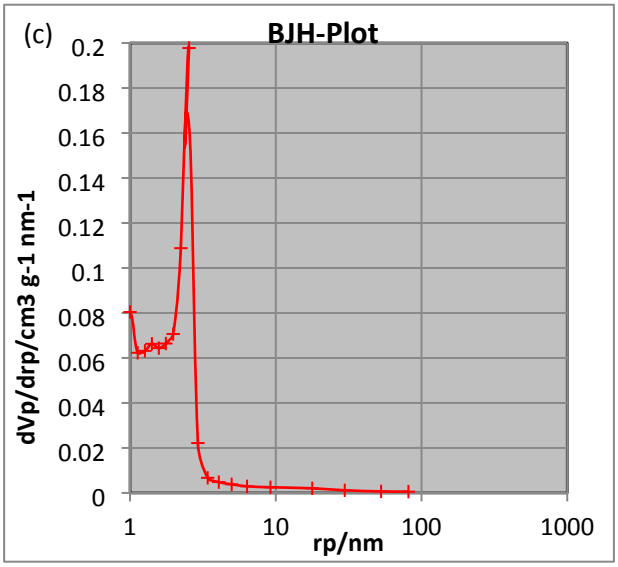

View Article Online
DOI: 10.1039/D5NA00548B

Fig. 7 N_2 adsorption–desorption isotherms for β-CD-bis-APTS (a) and β-CD-APTS-PMO (b); BJH pore size distributions for β-CD-APTS-PMO (c).

Investigation of curcumin and paclitaxel loading

Paclitaxel and curcumin were selected as two model drugs in the treatment of lung cancer in this study. In this regard, the amount of 0.2 g of β-CD-APTS-PMO was added to the solutions containing the drug and it was stirred for 24 h at room temperature. Then, drug loaded β-CD-APTS-PMO was separated and dried with vacuum oven. In next, the supernatant solution was analysed with UV-Vis and the percentage of loading capacity and entrapment efficiency was calculated using the primary and secondary concentrations.

According to articles, specific FTIR peaks for paclitaxel and curcumin were determined in **Fig. 8**. Some of the characteristic peaks of curcumin including 1628 cm^{-1} (aromatic moiety C=C stretching), 1605 cm^{-1} (benzene ring stretching), 1511 cm^{-1} (C=O and C=C vibrations), 1430 cm^{-1} (olefinic C-H bending), 1280 cm^{-1} (aromatic C–O stretching) and 1024 cm^{-1} (C–O–C stretching) were located at or shifted to 1620, 1606, 1517 and 1431 cm^{-1}, respectively, in the FTIR spectrum of CUR-β-CD-APTS-PMO (**Fig. 8d**). Paclitaxel showed its typical peaks at 1736 (C=O stretching), 1647 (C–C stretching) 1370 (CH_3 deformation) 1247 (C–N stretching) 1074 (C–O stretching), which some of them were located at or shifted to 1736, 1641 and 1370 cm^{-1}, respectively, in the FTIR spectrum of PTX-β-CD-APTS-PMO.[78] Finally, in the FTIR spectrum of PTX/CUR-β-CD-APTS-PMO, the peaks at 1740, 1647 and 1370 cm^{-1} were attributed to the overlap of C=O stretching, C–C stretching and CH_3 deformation of PTX, respectively. Furthermore, the peaks at 1625, 1511 and 1432 cm^{-1} were assigned to the overlap of aromatic moiety C=C stretching, C=O and C=C vibrations and olefinic C–H bending of curcumin, respectively.[79, 80] The shifting of peaks in the FTIR spectrum upon PTX and CUR loading into the β-CD-APTS-PMO confirms molecular interactions that have occurred between the drugs and the carrier. These shifts are due to the changes in vibrational energy of the functional groups within drug molecules (paclitaxel and curcumin) and the carrier material, which is a direct consequence of new or altered intermolecular forces. Indeed, hydrogen bonding is significant cause of peak shifts, especially for molecules such as paclitaxel and curcumin, which have multiple hydroxyl (O–H) and carbonyl (C=O) groups. When a strong H-bond is formed, the vibrating bond is weakened and its effective mass is increased. The shifts of peaks confirm that the drugs are not just a physical mixture with the carrier but they have been successfully incorporated and are interacting at a molecular level, indicating effective loading.

Table 1 Entrapment efficiency and drug loading capacity of β-CD-bis-APTS and β-CD-APTS-PMO for PTX and CUR (mean ± SD, n = 3)

Drug Solution	Nanocarrier	Initial concentration of drug	Initial amount of drug	Remained drug concentration in the solution	Remained drug amount in the solution	Amount of loaded drug	LC (%)	EE (%)
CUR	β-CD-bis-APTS	500 µg/mL	10 mg	268 µg/mL	5.36 mg	4.64 mg	23.2 ± 0.014	46.4 ± 0.28
PTX	β-CD-bis-APTS	500 µg/mL	10 mg	282 µg/mL	5.64 mg	4.36 mg	21.8 ± 0.032	43.6 ± 0.64
CUR / PTX	β-CD-bis-APTS	500 µg/ mL / 500 µg/mL	10 mg 10 mg	270 µg/mL / 286 µg/mL	5.4 mg / 5.72 mg	4.6 mg / 4.28 mg	23.0 ± 0.07 / 21.4± 0.011	46.0 ± 0.14 / 42.8 ± 0.21
CUR	β-CD-APTS-PMO	500 µg/mL	10 mg	47 µg/mL	0.96 mg	9.04 mg	45.2 ± 0.035	90.4 ± 0.71
PTX	β-CD-APTS-PMO	500 µg/mL	10 mg	61 µg/mL	1.22 mg	8.78 mg	43.9 ± 0.017	87.8 ± 0.34
CUR / PTX	β-CD-APTS-PMO	500 µg/mL / 500 µg/mL	10 mg 10 mg	49 µg/mL / 63 µg/mL	0.98 mg / 1.26 mg	9.02 mg / 8.74 mg	45.1 ± 0.028 / 43.7 ± 0.06	90.2 ± 0.56 / 87.4 ± 0.12

Nanoscale Advances

ARTICLE

View Article Online
DOI: 10.1039/D5NA00544B

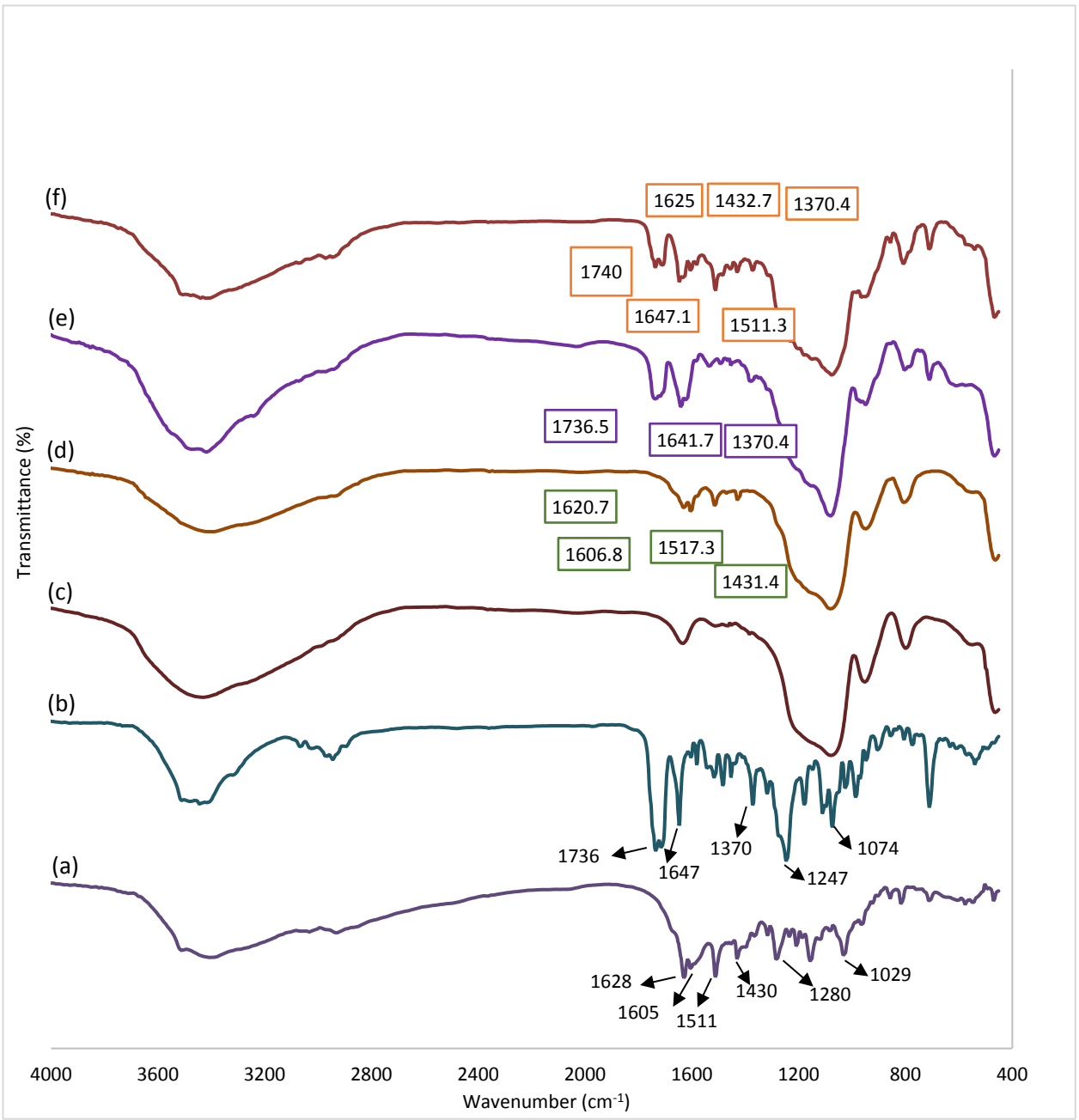

Fig. 8 FT-IR spectra of curcumin (a), PTX(b), β-CD-APTS-PMO (c), CUR-β-CD-APTS-PMO (d), PTX-β-CD-APTS-PMO (e), PTX/CUR-β-CD-APTS-PMO (f).

DLS and zeta potential

The physicochemical characteristics of β-CD-APTS-PMO, CUR-β-CD-APTS-PMO, PTX-β-CD-APTS-PMO and PTX/CUR-β-CD-APTS-PMO including particle size, polydispersity index (PDI) and zeta potential are shown in **Table 2**. β-CD-APTS-PMO demonstrated the smaller particle size of 27.86 ± 0.31 compared to 54.63 ± 0.51 or 57.84 ± 0.26 for CUR-β-CD-APTS-PMO or PTX-β-CD-APTS-PMO, respectively.

Table 2 Particle size, poly dispersity index and zeta potential of drug-free and drug-loaded β-CD-APTS-PMO (mean ± SD, n = 3)

Formulation	Particle size (nm ± SD)	Potential zeta (mV)	PDI ± SD
β-CD-APTS-PMO	27.86 ± 0.31	+15.7	0.61 ± 0.21
CUR-β-CD-APTS-PMO	54.63 ± 0.51	+36.8	0.567 ± 0.34
PTX-β-CD-APTS-PMO	57.84 ± 0.26	+42.5	0.621 ± 0.17
PTX/CUR-β-CD-APTS-PMO	68.42 ± 0.13	+45.3	0.803 ± 0.23

In vitro pH-responsive release of curcumin

In vitro PTX and CUR release behaviours of CUR-β-CD-APTS-PMO, PTX-β-CD-APTS-PMO, PTX/CUR-β-CD-APTS-PMO were performed using PBS at two different pH values (7.4 and 5.5) at 37 °C and data are shown in **Fig. 9**. At first, the release profile of CUR-β-CD-APTS-PMO and PTX-β-CD-APTS-PMO were investigated and subsequently compared with PTX/CUR-β-CD-APTS-PMO. At pH 7.4, almost 37% and 26% of the curcumin and paclitaxel were released from CUR-β-CD-APTS-PMO, PTX-β-CD-APTS-PMO after 72 h, respectively. As well, 66% and 58% of the curcumin and paclitaxel were released after 24 h and increased to 78% and 66% after 72 h in pH 5.5, respectively. Furthermore, in vitro release profiles of CUR and PTX from the co-delivery system have been displayed in **Fig. 9b**. The amount of released CUR and PTX was approximately 75% and 53% up to 24 h in pH 5.5, respectively. Then, drug release reaching around 87% and 68% in 72 h. Eventually, about 35% and 24% of the CUR and PTX was released within 36 h in pH 7.4 and being this level remained after 72 h. According to results, the release profiles illustrated that CUR can be released earlier and faster than PTX, which is more hydrophobic. In addition, slow drug release behaviour was attributable to the entrapment of CUR and PTX in the β-cyclodextrin and PMO pores.

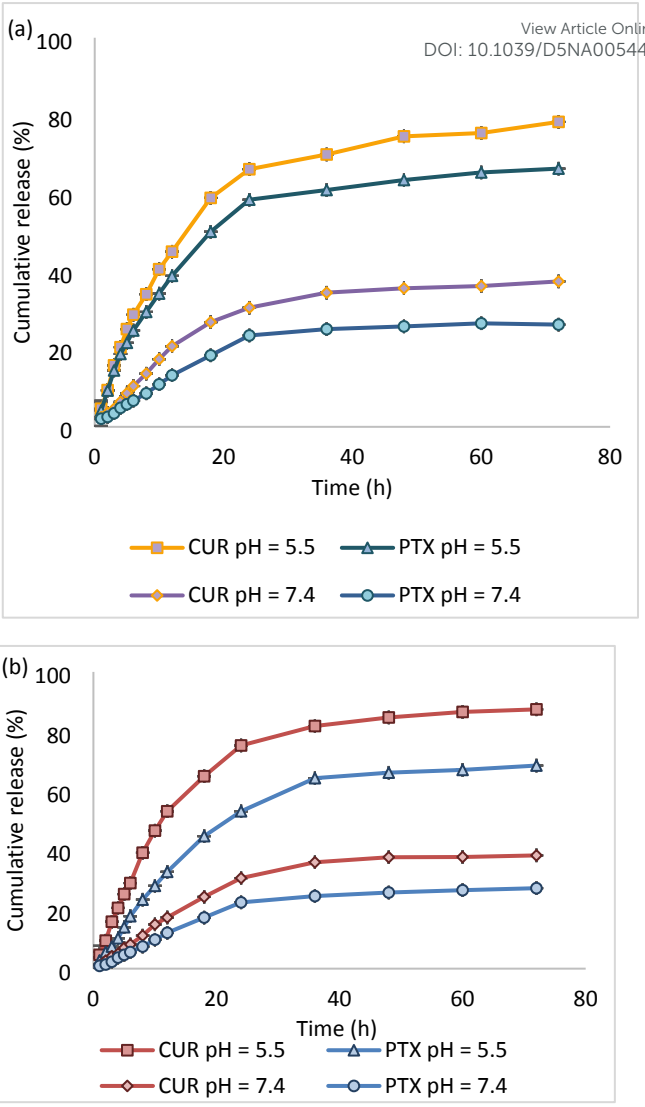

Fig. 9 The drug release curve at pH = 7.4 and 5.5 from PTX-loaded and CUR-loaded β-CD-APTS-PMO and (a) PTX/CUR-loaded β-CD-APTS-PMO (b) (mean ± SD, n = 3).

Release kinetics of CUR and PTX from β-CD-APTS-PMO in various media (pH 7.4 and 5.5) were investigated by fitting experimental data to four common release models. Comparison of R2 values revealed that both Higuchi and Korsmeyer-Peppas models best described the release kinetics in both media. Furthermore, the experimental kinetic models indicated non-Fickian CUR and PTX release in both media. The established diagram representations and obtained results are respectively depicted in **Fig. S10 - 17** and summarized in **Table 3**.

MTT assay

The effects of different concentration of drugs and drug-loaded β-CD-APTS-PMO against A549 cells were detected by MTT assay. In this regard, CUR, PTX, β-CD-APTS-PMO, CUR-β-CD-APTS-PMO, PTX-β-CD-APTS-PMO and PTX/CUR-β-CD-APTS-PMO exhibited a dose-

dependent cytotoxicity in the cell lines tested. β-CD-APTS-PMO showed about 88% cell viability at high concentration after 48 h, which revealed its biocompatible property. Results showed that the effect of toxicity increases by increasing the concentration of each drug. Cytotoxicity of PTX was relatively more than that of CUR (the average is about 10 percent) which could be probably due to the higher hydrophobicity of PTX leading to more endocytosis into the cell. In A549 cells, the IC50 of PTX was 40.45 μg/mL, while the IC50 was 28.40 μg/mL for PTX-loading β-CD-APTS-PMO after 48 h. CUR had an IC50 of 59.57 μg/mL and the IC50 of CUR -loading β-CD-APTS-PMO was 33.91 μg/mL. When both PTX and CUR were loaded in the β-CD-APTS-PMO, the IC50 was smaller (19.78 μg/mL) and showed a higher antiproliferative effect on A549 cells, indicating that the two drugs have a synergistic effect.

Table 3 Mathematical results of the CUR and PTX release fitting with kinetic equations

Kinetic release models	Equation	CUR-β-CD-APTS-PMO		PTX-β-CD-APTS-PMO		PTX/CUR-β-CD-APTS-PMO	
		pH = 7.4	pH = 5.5	pH = 7.4	pH = 5.5	pH = 7.4 (CUR) (PTX)	pH = 5.5 (CUR) (PTX)
Zero order	$Q = k_0t$	$K_0 = 0.5142$	$K_0 = 0.9915$	$K_0 = 0.3781$	$K_0 = 0.777$	$K_0 = 0.5688$ $K_0 = 0.4023$	$K_0 = 1.1515$ $K_0 = 0.9859$
		$R^2 = 0.7942$	$R^2 = 0.775$	$R^2 = 0.8018$	$R^2 = 0.8552$	$R^2 = 0.8336$ $R^2 = 0.8328$	$R^2 = 0.7641$ $R^2 = 0.831$
First order	$LnQ = LnQ_0 - k_1t$	$K_1 = 0.0447$	$K_1 = 0.0385$	$K_1 = 0.0452$	$K_1 = 0.0373$	$K_1 = 0.0535$ $K_1 = 0.0549$	$K_1 = 0.041$ $K_1 = 0.0496$
		$R^2 = 0.5929$	$R^2 = 0.5279$	$R^2 = 0.6378$	$R^2 = 0.5303$	$R^2 = 0.5918$ $R^2 = 0.6026$	$R^2 = 0.5258$ $R^2 = 0.5958$
Higuchi model	$Q = k_Ht^{1/2}$	$K_H = 5.2967$	$K_H = 10.298$	$K_H = 3.8734$	$K_H = 8.7313$	$K_H = 5.7806$ $K_H = 4.0863$	$K_H = 11.993$ $K_H = 10.047$
		$R^2 = 0.9233$	$R^2 = 0.916$	$R^2 = 0.9219$	$R^2 = 0.9119$	$R^2 = 0.9433$ $R^2 = 0.9412$	$R^2 = 0.9082$ $R^2 = 0.9453$
Korsmeyer's–Peppas	$LnQ = nLnt + Lnk_p$	$N = 0.6934$	$N = 0.8751$	$N = 0.68$	$N = 0.7406$	$N = 0.8339$ $N = 0.8483$	$N = 0.9853$ $N = 0.9612$
		$R^2 = 0.945$	$R^2 = 0.981$	$R^2 = 0.958$	$R^2 = 0.9588$	$R^2 = 0.9518$ $R^2 = 0.9525$	$R^2 = 0.9954$ $R^2 = 0.9929$

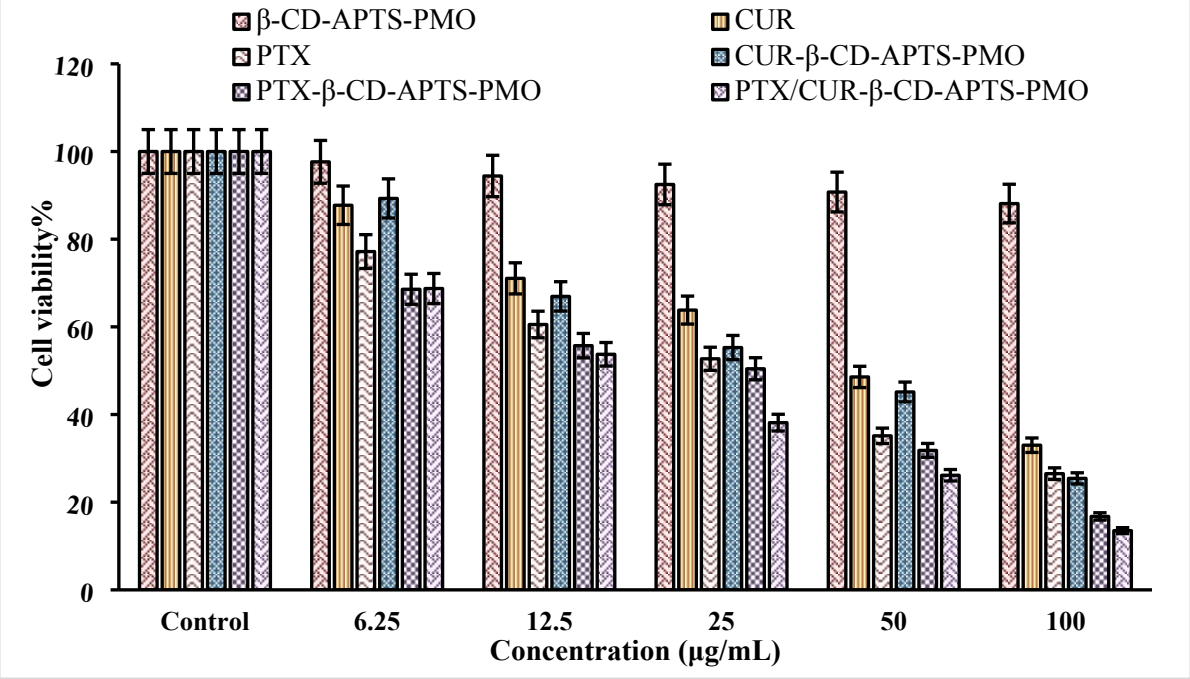

Fig. 10 In vitro cytotoxicity analysis of curcumin, PTX, β-CD-APTS-PMO, CUR-β-CD-APTS-PMO, PTX-β-CD-APTS-PMO and PTX/CUR-β-CD-APTS-PMO against A549 cell line.

Nanoscale Advances

View Article Online
DOI: 10.1039/D5NA00544B

ARTICLE

Comparison of β-CD-APTS-PMO and other CUR/PTX combination delivery systems

Recently, various types of nanomaterials have been studied to CUR/PTX combination delivery, including polymers, graphene oxide, hybrid nanomaterials and liposomes.[81] Meanwhile, mesoporous organosilica materials can lead to higher encapsulation of large amounts of therapeutic agents due to their high pore sizes, surface areas, and pore volumes. In this regard, the capability and efficiency of drug loading and release by β-CD-APTS-PMO nanocarrier and some recent CUR/PTX delivery systems is compared in **Table 4**.

Table 4 Comparative results of different nanocarriers for CUR/PTX delivery

No	Drug carrier	EE (%)	Duration of release (h)	Max amount release	Cell-tested	IC50	Cell viability	Ref
1	FPCN	79.1 ± 4.2 (PTX) 85.7 ± 5.2 (CUR)	48 h	~ 80%	MCF-7/ ADR cells	-	~ >20%	82
2	PCEC copolymer	92.6 ± 4.42 (PTX) 90.3 ± 1.44 (CUR)	8 days	82.78% (PTX) 80% (CUR)	MCF-7 cells	-	~ 50%	83
3	BPGNRs	85.3 ± 1.53 (PTX) 85.0 ± 1.86 (CUR)	72 h	49.89 ± 1.78% (PTX) 51.65 ± 2.37% (CUR)	MCF-7 /ADR cells	5.65 µg/mL (PTX) 12.98 µg/mL (CUR)	~ 70%	84
4	GO-PF-127 (GP)	96.56 ± 0.07	96 h	~ 30% (PTX) ~ 70% (CUR)	A549 and MDA cells	13.24 µg/mL (A549 cell) 1.450 µg/mL (MDA cell)	~ 40% (A549 cell) ~ 30% (MDA cell)	85
5	PLMSNs	77.48 ± 2.73 (PTX) 30.70 ± 3.56 (CUR)	96 h	52.07% (PTX)	canine breast cancer cells	0.19 µg/mL (PTX) 53.16 µg/mL (CUR)	~ 30%	65
6	β-CD-APTS-PMO	87.4 ± 0.12 (PTX) 90.2 ± 0.56 (CUR)	72 h	~ 68% (PTX) ~ 87% (CUR)	A549 cells	33.90 µg/mL (CUR) 28 .40 µg/mL (PTX) 19.78 µg/mL (PTX /CUR)	13.51%	This study

Conclusions

In this study, we designed and synthesized β-cyclodextrin grafted to 3-aminopropyl group and incorporated into the periodic mesoporous organosilica structure (β-CD-APTS-PMO), as a controllable drug delivery vehicle, which enables pH-responsive release of encapsulated model CUR and PTX chemotherapeutic agents. To the best of our knowledge, this is the first report of incorporating of β-cyclodextrin into the PMO structure as a stimulus responsive drug release system. The incorporation of β-CD into PMO hybrid materials increases guest-host interactions and improved solubility. In addition, this

exceptional design not only provided a stable and rigid framework by uniform and tunable pore size, high surface area as well as high pore volumes, but can also effectively increased encapsulation efficiency (CUR: 90.2 ± 0.56%, PTX: 87.4 ± 0.12%) and control release (CUR: 87%, PTX: 68%) in the intracellular environment of cancer cells. Moreover, the administration of PTX/CUR-β-CD-APTS-PMO to A549 cells exhibited dose dependent toxicity (IC50: 19.78 µg/mL) as compared to the control experiment. In general, this design might have important implications for future development of mesoporous but controllable smart drug delivery systems, which might be beneficial for precise treatment of lung cancer.

Author contributions

Negin Rostami: Methodology, Software, Formal analysis, Investigation, Data Curation, Writing - Original Draft; **Mohammad Reza Naimi-Jamal:** Conceptualization; Methodology, Validation, Resources, Data Curation, Writing - Review & Editing; **Mohammad G. Dekamin:** Conceptualization, Methodology, Validation, Resources, Data Curation, Writing - Review & Editing.

Conflicts of interest

There are no conflicts to declare.

Acknowledgements

We are grateful acknowledge for the financial support from The Research Council of Iran University of Science and Technology (IUST), Tehran, Iran. The partial financial support of the Iran Nanotechnology Initiative Council (INIC) is also highly appreciated.

Notes and references

1. B. Yang, Y. Chen and J. Shi, *Materials Science and Engineering: R: Reports*, 2019, **137**, 66-105.
2. X. Du, X. Li, L. Xiong, X. Zhang, F. Kleitz and S. Z. Qiao, *Biomaterials*, 2016, **91**, 90-127.
3. C. M. Jimenez, N. Z. Knezevic, Y. G. Rubio, S. Szunerits, R. Boukherroub, F. Teodorescu, J. G. Croissant, O. Hocine, M. Seric and L. Raehm, *Journal of Materials Chemistry B*, 2016, **4**, 5803-5808.
4. B. Karimi, N. Ganji, O. Pourshiani and W. R. Thiel, *Progress in Materials Science*, 2022, **125**, 100896.
5. A. M. Kaczmarek, S. Abednatanzi, D. Esquivel, C. Krishnaraj, H. S. Jena, G. Wang, K. Leus, R. Van Deun, F. J. Romero–Salguero and P. Van Der Voort, *Microporous and Mesoporous Materials*, 2020, **291**, 109687.
6. A. Akbari, M. G. Dekamin, A. Yaghoubi and M. R. Naimi-Jamal, *Scientific Reports*, 2020, **10**, 10646.
7. E. Valiey and M. G. Dekamin, *Nanoscale Advances*, 2022, **4**, 294-308.
8. A. Zebardasti, M. G. Dekamin, E. Doustkhah and M. H. N. Assadi, *Inorganic Chemistry*, 2020, **59**, 11223-11227.
9. A. Eftekhari, M. Dalili, Z. Karimi, S. Rouhani, A. Hasanzadeh, S. Rostamnia, S. Khaksar, A. O. Idris, H. Karimi-Maleh and M. L. Yola, *Food Chemistry*, 2021, **358**, 129763.
10. I. Diédhiou, A. Sebei, M. Fall, S. B. Aoun, R. Zarrougui and N. Raouafi, *Electroanalysis*, 2023, **35**, e202300072.
11. X. Feng, F. Li, L. Zhang, W. Liu, X. Wang, R. Zhu, Z.-A. Qiao, B. Yu and X. Yu, *Acta biomaterialia*, 2022, **143**, 392-405.
12. T. Shao, J. Wen, Q. Zhang, Y. Zhou, L. Liu, L. Yuwen, Y. Tian, Y. Zhang, W. Tian and Y. Su, *Journal of Materials Chemistry B*, 2016, **4**, 7708-7717.
13. E. Doustkhah, H. Mohtasham, M. Hasani, Y. Ide, S. Rostamnia, N. Tsunoji and M. H. N. Assadi, *Molecular Catalysis*, 2020, **482**, 110676.
14. A. Yaghoubi, M. G. Dekamin, E. Arefi and B. Karimi, *J. Colloid Interface Sci.*, 2017, **505**, 956-963.
15. H. Fanimoghadam, M. G. Dekamin and M. R. Naimi-Jamal, *Nanoscale Advances*, 2025, **7**, 4691-4709.
16. B. Q. G. Le and T. L. H. Doan, *Wiley Interdisciplinary Reviews: Nanomedicine and Nanobiotechnology*, 2023, **15**, e1874.
17. S. Zhou, Q. Zhong, Y. Wang, P. Hu, W. Zhong, C.-B. Huang, Z.-Q. Yu, C.-D. Ding, H. Liu and J. Fu, *Coordination Chemistry Reviews*, 2022, **452**, 214309.
18. R. Khoz, F. Yazdian, M. Pourmadadi, A. Rahdar, S. Fathi-karkan and S. Pandey, *European Journal of Medicinal Chemistry Reports*, 2024, 100206.
19. A. Motealleh, P. Dorri and N. S. Kehr, *Journal of Materials Chemistry B*, 2019, **7**, 2362-2371.
20. N. Wu, X. Zeng, B. Liu, F. X. Song, M. L. Chen, X. Q. Cai, H. H. Luo and Y. Li, *Journal of Drug Delivery Science and Technology*, 2023, **80**, 104102.
21. R. S. Guimarães, C. F. Rodrigues, A. F. Moreira and I. J. Correia, *Pharmacological Research*, 2020, **155**, 104742.
22. N. Lu, Y. Tian, W. Tian, P. Huang, Y. Liu, Y. Tang, C. Wang, S. Wang, Y. Su and Y. Zhang, *ACS applied materials & interfaces*, 2016, **8**, 2985-2993.
23. Z. Shariatinia, *Journal of Drug Delivery Science and Technology*, 2021, **66**, 102790.
24. K. Živojević, M. Mladenović, M. Djisalov, M. Mundzic, E. Ruiz-Hernandez, I. Gadjanski and N. Ž. Knežević, *Journal of Controlled Release*, 2021, **337**, 193-211.
25. A. Motealleh, R. De Marco and N. S. Kehr, *Journal of Materials Chemistry B*, 2019, **7**, 3716-3723.
26. N. Ahmed and Z. N. Siddiqui, *RSC Advances*, 2015, **5**, 16707-16717.
27. X. Qian, W. Wang, W. Kong and Y. Chen, *Journal of Nanomaterials*, 2014, **2014**, 972475.
28. S. Parambadath, A. Mathew, M. J. Barnabas and C.-S. Ha, *Microporous and Mesoporous Materials*, 2015, **215**, 67-75.
29. Y. GÖK, H. Z. GÖK, O. T. ARLI and T. TÜRKASLAN, *Turkish Journal of Chemistry*, 2025, **49**, 439-449.
30. W. Zhang, H. Ma, J. Hua, W. Zhang, C. Guo and J. Wang, *J. Solid State Chem.*, 2019, **277**, 761-768.
31. K. M. Rao, S. Parambadath, A. Kumar, C.-S. Ha and S. S. Han, *ACS Biomaterials Science & Engineering*, 2018, **4**, 175-183.
32. P. R. Salekdeh, L. Ma'mani, J. Tavakkoly-Bazzaz, H. Mousavi, M. H. Modarressi and G. H. Salekdeh, *Journal of Nanobiotechnology*, 2021, **19**, 95.
33. N. X. D. Mai, T.-H. T. Nguyen, L. H. T. Nguyen, H. T. Nguyen, T. B. Phan, F. Tamanoi, L. B. Vong and T. L. H. Doan, *Colloids and Surfaces A: Physicochemical and Engineering Aspects*, 2023, **656**, 130405.

34. R. Xing, L. Ning, L. Li, L. He, H. Lin, C. You and F. Wang, *Journal of Drug Delivery Science and Technology*, 2023, **86**, 104654.
35. S. Datz, H. Engelke, C. V. Schirnding, L. Nguyen and T. Bein, *Microporous and mesoporous materials*, 2016, **225**, 371-377.
36. A. Roy, K. Manna, S. Dey and S. Pal, *Carbohydrate Polymers*, 2023, **306**, 120576.
37. F. Calsolaro, F. Garello, E. Cavallari, G. Magnacca, M. V. Trukhan, M. C. Valsania, G. Cravotto, E. Terreno and K. Martina, *Nanoscale Advances*, 2025, **7**, 155-168.
38. R. Biswas, S. Yang, R. A. Crichton, P. Adly-Gendi, T. K. Chen, W. P. Kopcha, Z. Shi and J. Zhang, *Nanoscale*, 2022, **14**, 4456-4462.
39. K. M. Sahu, S. Patra and S. K. Swain, *Int. J. Biol. Macromol.*, 2023, **240**, 124338.
40. N. Wang, Y. Liu, Y. Wu, Z. Li and D. Wang, *Nanoscale Advances*, 2021, **3**, 6063-6073.
41. M. A. Fernández, O. F. Silva, R. V. Vico and R. H. de Rossi, *Carbohydrate research*, 2019, **480**, 12-34.
42. P. Mura, *International journal of pharmaceutics*, 2020, **579**, 119181.
43. S. Amiri and S. Amiri, *Micro-and Nano-containers for Smart Applications*, 2022, 327-357.
44. G. Fang, X. Yang, S. Chen, Q. Wang, A. Zhang and B. Tang, *Coordination Chemistry Reviews*, 2022, **454**, 214352.
45. J. Wang, G. Liu, C. Zhou, X. Cui, W. Wang, J. Wang, Y. Huang, J. Jiang, Z. Wang and Z. Tang, *Nanoscale*, 2024, **16**, 14213-14246.
46. R. Sharma, *International Journal of Clinical Oncology*, 2022, **27**, 665-675.
47. L. Zhong, Y. Li, L. Xiong, W. Wang, M. Wu, T. Yuan, W. Yang, C. Tian, Z. Miao and T. Wang, *Signal transduction and targeted therapy*, 2021, **6**, 1-48.
48. Y. Chen, Q. Zhang, J. Shen, Z. Liu, X. Cui, L. Ma, Y. Zheng, L. Wang and T. Ying, *Journal of Colloid and Interface Science*, 2025, **678**, 108-118.
49. B. Honarvari, S. Karimifard, N. Akhtari, M. Mehrarya, Z. S. Moghaddam, M. J. Ansari, A. T. Jalil, A. Matencio, F. Trotta, F. E. Yeganeh, B. Farasati Far, M. K. Arki, M. R. Naimi-Jamal, H. Noorbazargan, Z. A. Lalami and M. Chiani, *Molecules*, 2022, **27**, 4634.
50. C. Pi, W. Zhao, M. Zeng, J. Yuan, H. Shen, K. Li, Z. Su, Z. Liu, J. Wen and X. Song, *Drug Delivery*, 2022, **29**, 1878-1891.
51. J. Riedel, M. N. Calienni, E. Bernabeu, V. Calabro, J. M. Lázaro-Martinez, M. J. Prieto, L. Gonzalez, C. S. Martinez, S. del Valle Alonso and J. Montanari, *Journal of Drug Delivery Science and Technology*, 2021, **62**, 102343.
52. M. Baroud, E. Lepeltier, S. Thepot, Y. El-Makhour and O. Duval, *Nanoscale Advances*, 2021, **3**, 2157-2179.
53. M. Pourmadadi, P. Abbasi, M. M. Eshaghi, A. Bakhshi, A.-L. E. Manicum, A. Rahdar, S. Pandey, S. Jadoun and A. M. Díez-Pascual, *Journal of Drug Delivery Science and Technology*, 2022, **78**, 103982.
54. M. K. Zenjanab, S. Alimohammadvand, A. Doustmihan, S. Kianian, B. S. Oskouei, M. Mazloomi, M. Akbari and R. Jahanban-Esfahlan, *Journal of Drug Delivery Science and Technology*, 2024, 105567.
55. H. Herman, D. M. Rata, A. N. Cadinoiu, L. I. Atanase and A. Hermenean, *Polymers*, 2024, **16**, 1189.
56. A. M. Khalifa, M. A. Elsheikh, A. M. Khalifa and Y. S. Elnaggar, *Journal of Controlled Release*, 2019, **311**, 125-137.
57. J. Sharifi-Rad, C. Quispe, J. K. Patra, Y. D. Singh, M. K. Panda, G. Das, C. O. Adetunji, O. S. Michael, O. Sytar and L. Polito, *Oxidative medicine and cellular longevity*, 2021, **2021**, 3687700.
58. Y.-S. Fu, T.-H. Chen, L. Weng, L. Huang, D. Lai and C.-F. Weng, *Biomedicine & Pharmacotherapy*, 2021, **141**, 111888.
59. Y. Peng, S. Yu, Z. Wang, P. Huang, W. Wang and J. Xing, *Journal of Materials Chemistry B*, 2022, **10**, 3293-3302.
60. Y. Cao, R. Xu, Y. Liang, J. Tan, X. Guo, J. Fang, S. Wang and L. Xu, *Nanoscale*, 2024, **16**, 13718-13754.
61. M. Ashrafizadeh, A. Zarrabi, F. Hashemi, E. R. Moghadam, F. Hashemi, M. Entezari, K. Hushmandi, R. Mohammadinejad and M. Najafi, *Life sciences*, 2020, **256**, 117984.
62. T. Saghatelyan, A. Tananyan, N. Janoyan, A. Tadevosyan, H. Petrosyan, A. Hovhannisyan, L. Hayrapetyan, M. Arustamyan, J. Arnhold and A.-R. Rotmann, *Phytomedicine*, 2020, **70**, 153218.
63. X. Lin, Q. Wang, S. Du, Y. Guan, J. Qiu, X. Chen, D. Yuan and T. Chen, *Journal of Drug Delivery Science and Technology*, 2023, **79**, 104050.
64. C. L. Barrera-Martínez, H. I. Meléndez-Ortiz, F. Padilla-Vaca, L. I. dease, R. D. Peralta-Rodríguez and I. Liakos, *Polymers*, 2024, **16**, 3087.
65. J. Lin, Q. Cai, Y. Tang, Y. Xu, Q. Wang, T. Li, H. Xu, S. Wang, K. Fan and Z. Liu, *International Journal of Pharmaceutics*, 2018, **536**, 272-282.
66. H. Hu, Z. Liao, M. Xu, S. Wan, Y. Wu, W. Zou, J. Wu and Q. Fan, *ACS omega*, 2022, **8**, 976-986.
67. C. Pacheco, A. Baiao, T. Ding, W. Cui and B. Sarmento, *Advanced Drug Delivery Reviews*, 2023, **194**, 114724.
68. B. G. Carvalho, F. F. Vit, H. F. Carvalho, S. W. Han and L. G. de la Torre, *Journal of Materials Chemistry B*, 2021, **9**, 1208-1237.
69. J. Liu, L. Li, B. Zhang and Z. P. Xu, *Journal of Colloid and Interface Science*, 2022, **617**, 315-325.
70. Z. Xu, S. Liu, Y. Kang and M. Wang, *Nanoscale*, 2015, **7**, 5859-5868.
71. F. Shahidi, M. R. Naimi-Jamal, A. Habibi and M. G. Dekamin, *Current Drug Delivery*, 2025, **22**, 583-592.
72. E. Valiey and M. G. Dekamin, *RSC Advances*, 2022, **12**, 437-450.
73. M. Tajbakhsh and M. R. Naimi-Jamal, *Scientific Reports*, 2022, **12**, 4948.
74. K. Liu, H. Liu, Z. Li, W. Li and L. Li, *Journal of inclusion phenomena and macrocyclic chemistry*, 2020, **96**, 233-243.
75. Z. A. Haiyee, N. I. A. Yahya, N. Rashid and D. M. Hashim, *Malaysian Journal of Analytical Sciences*, 2016, **20**, 838-843.
76. A. Saifi, J. P. Joseph, A. P. Singh, A. Pal and K. Kumar, *ACS omega*, 2021, **6**, 4776-4782.
77. A. Svidrytski, D. Hlushkou, M. Thommes, P. A. Monson and U. Tallarek, *The Journal of Physical Chemistry C*, 2020, **124**, 21646-21655.
78. T. R. Devi and S. Gayathri, *Int J Pharm Sci Rev Res*, 2010, **2**, 106-110.
79. M. A. Chaves and S. C. Pinho, *Food chemistry*, 2019, **291**, 7-15.

80. X. Chen, L.-Q. Zou, J. Niu, W. Liu, S.-F. Peng and C.-M. Liu, *Molecules*, 2015, **20**, 14293-14311.
81. H. Batra, S. Pawar and D. Bahl, *Pharmacological Research*, 2019, **139**, 91-105.
82. J.-S. Baek and C.-W. Cho, *Oncotarget*, 2017, **8**, 30369.
83. K. Xiong, Y. Zhang, Q. Wen, J. Luo, Y. Lu, Z. Wu, B. Wang, Y. Chen, L. Zhao and S. Fu, *International journal of pharmaceutics*, 2020, **589**, 119875.
84. S. Xu, Z. Jin, Z. Zhang, W. Huang, Y. Shen, Z. Wang and S. Guo, *Journal of Drug Delivery Science and Technology*, 2019, **54**, 101383.
85. K. Muthoosamy, I. B. Abubakar, R. G. Bai, H.-S. Loh and S. Manickam, *Scientific reports*, 2016, **6**, 32808.

View Article Online
DOI: 10.1039/D5NA00544B

Data Availability Statement

pH-Sensitive β-cyclodextrin-PMO hybrid nanomaterial for co-delivery of paclitaxel and curcumin in lung cancer

Negin Rostami,[a,b] Mohammad Reza Naimi-Jamal*[a] and Mohammad G. Dekamin*[b]

The data supporting this article have been included as part of the Supplementary Information.